ToF-SIMS depth profiling of altered glass

Marie Collin, S. Gin, Patrick Jollivet, Laurent Dupuy, Vincent Dauvois, Laurent Duffours

npj | Materials Degradation

www.nature.com/npjmatdeg

ARTICLE OPEN

ToF-SIMS depth profiling of altered glass

Marie Collin[1], Stéphane Gin[1], Patrick Jollivet[1], Laurent Dupuy[2], Vincent Dauvois[3] and Laurent Duffours[4]

Glass and mineral corrosion usually leads to the formation of morphologically and compositionally complex surface layers that can be characterized by various analytical techniques to infer rate control mechanisms. In this study, we investigate the capabilities and limitations of time-of-flight secondary ion mass spectrometry (ToF-SIMS) to better understand chemical processes of glass corrosion. In particular, we focus on the potential impact of the ToF-SIMS ion beam on the distribution of several elements of interest in alteration layers formed on International Simple Glass, a six-oxide reference glass altered in a solution enriched in alkalis and spiked with $H_2{}^{18}O$. A thin flake of glass partially altered on both sides is analyzed entirely from one side to the other to determine whether atoms weakly bonded to the solid are displaced by the beams. We highlight the beam effect on cations weakly bonded to the silicate network (Li, Na, K, and B, Ca, Cs to a lesser extent) affecting the profile shape of these elements. No impact is observed on ^{18}O and H, but it is demonstrated that quantification of isotopic ratios is possible only for a limited range of isotopic enrichment.

npj Materials Degradation (2019)3:14 ; https://doi.org/10.1038/s41529-019-0076-3

INTRODUCTION

Secondary ion mass spectrometry (SIMS) is a powerful, isotope sensitive, analytical tool for surfaces, and sub-surfaces characterization. It has been used since its development to detect nearly all elements of the periodic table regardless of their weight, even as trace elements.[1] During SIMS analysis, a focused primary ion beam hit the sample surface, resulting in the production of secondary ions from the sample surface that can be collected for mass spectrometry analysis.[2] Various SIMS modes currently exist, each with their advantages and limitations. Time-of-flight secondary ion mass spectrometry (ToF-SIMS) for example has a good depth resolution (potentially < 1 nm), better than that of dynamic secondary ion mass spectrometry (D-SIMS), but is less sensitive.[1] Nano-SIMS analysis provides the best lateral resolution, but this is obtained at the expense of depth resolution. Furthermore, Nano-SIMS analysis usually requires extensive sample preparation, while ToF-SIMS and D-SIMS can be applied directly on the sample surface (provided that its surface is flat). Despite ToF-SIMS lower sensitivity compared to D-SIMS, it is possible to use this technique with caution to characterize various types of layers. To take some examples, ToF-SIMS has been successfully applied to many scientific issues, such as medical research,[3–5] the polymer industry,[6] or space research.[7] ToF-SIMS depth profiling capacity is also particularly interesting for the corrosion community, because it facilitates the characterization of both pristine and altered materials, and allows the proposition of formation mechanisms for the latter.[8–15] In particular, silicate glass corrosion work is of great interest for heritage material conservation,[16,17] geochemistry,[18] and nuclear waste management.[19,20] Some examples are curators in museums who are confronted with patrimonial object degradation and conservation,[21,22] glass industries that aim to produce resistant glass composition for glassware[23] and building,[24] and medical applications that require highly soluble glasses for drug delivery.[25] Meanwhile, many countries such as France, Japan, the UK, and the USA have selected borosilicate glass as a confinement matrix for the most hazardous nuclear wastes. Within these communities, glass corrosion has been studied using a large array of analytical techniques, including SIMS.[26–30]

Glass corrosion often leads to the formation of multiple alteration layers, totally amorphous (called gel) or partially crystalline, including passivating and non-passivating films formed by coupled mechanisms (e.g., ion exchange, dissolution-reprecipitation, and/or partial hydrolysis-condensation of silicate species),[27,31–33] and secondary phases such as clay minerals, apatite, or zeolite.[15,34–36] D-SIMS,[1,26] nano-SIMS,[37–39] and Tof-SIMS[9,33–42] have all been used to characterize those layers, but these methods are not quantitative without calibration, as elemental ionization yields are matrix-dependent.[1] Nevertheless, provided that the matrix remains the same, semi-quantitative data can be obtained such as alteration layer thickness, composition, and homogeneity.[27,40] Interestingly, profile shapes at the pristine glass/gel interface can give insight into how the gel layer forms, as broad profiles are often associated with diffusion limiting processes, while a sharp interface can be the result of precipitation processes.[33,41,42] In addition, quantitative information regarding isotope ratio inside the layers—which give insight into layer formation as well—can also be obtained by SIMS.[1,26]

However, some uncertainties remain regarding ToF-SIMS depth profiling, limiting data interpretation. As an example, it was recently demonstrated that the size of the probed area impacts the profile width at the pristine glass/gel interface due to an increase in surface roughness.[12,42] This can be problematic, as the shape of the anti-correlated profiles of H and B is used to determine the diffusion coefficient of mobile species.[30,42–45] Furthermore, elemental normalized concentrations or isotopic ratios are generally plotted against depth after the measurement of the crater depth at the end of the analysis. This assumes that

[1]CEA, DEN, DE2D, SEVT, 30207 Bagnols-sur-Ceze, France; [2]Tescan Analytics, ZAC St Charles, 13710 Fuveau, France; [3]DEN-Service d'Etude du Comportement des Radionucléides, CEA, Université Paris-Saclay, 91191 Gif-sur-Yvette Cedex, France and [4]PRIME Verre, PAT du Millénaire bâtiment 10, 34000 Montpellier, France
Correspondence: Stéphane Gin (stephane.gin@cea.fr)

Received: 3 October 2018 Accepted: 13 March 2019
Published online: 02 April 2019

the abrasion rates of the different layers are the same or that they have been measured separately to correct the depth axis. While it has been demonstrated that abrasion rates are similar in pristine glass and passivating gels such as the ones formed in Si-saturation conditions,[11,27,31,46] they might differ in low-density secondary phases.[15] Consequently, uncertainties remain regarding the depth of each layer when displayed with no correction. Another potential concern not yet investigated is that the sputtering beam could impact the profile shape by displacing some elements such as alkali, oxygen, and hydrogen, especially in porous materials. In most gel layers, an increase in O and H intensities is indeed observed at the pristine glass/gel interface.[27,40] This increase could either be artificially induced by an accumulation of these species near the dense and uncorroded solid, or be a real feature of glass alteration. Similar uncertainties were investigated in other fields of study—thin film for photovoltaic cells or electronic integrated circuits—using backside SIMS analysis, i.e., the analysis of a sample from its back after removing most of its bulk material.[47–50]

In this study, the potential effects of sputtering on the elemental depth profiles are investigated in an analogous manner. The work is performed with the International Simple Glass (ISG), a six-oxide borosilicate glass of reference for the nuclear glass community.[51] A ~6 µm thick ISG glass flake was prepared and altered for a few days, a duration long enough to form a gel layer on both sides of the flake while still enclosing a pristine glass core. Due to the sample geometry, it was possible to avoid the usual preparation necessary for backside analysis (mainly chemical of physical etching of the bulk material).[48] The sample was then analyzed by ToF-SIMS from one side to another in a single shot. The results were two profiles obtained in opposite directions, which should be identical in the absence of artifacts. When compared, no effect was observed on the network former (Si, B, Zr). However, light mobile elements such as Li, Na, and K appear to have been pushed forward by the sputtering beam. This observation is confirmed by complementary analyses conducted on a cooled sample, maintaining the pore water frozen. Our findings indicate that uncertainties remain concerning some elemental depth profiles. With the selected analytical conditions, no effect was observed for O and H profiles, meaning that a mechanism can be inferred from the profiles of these elements in future glass corrosion studies.

RESULTS AND DISCUSSION

Analysis of the flake sample

The small thickness of the flake sample allowed its analysis in a single operation (from the first gel layer to the pristine glass core to the second gel layer, Fig. 8). In the following section, the flake sample profiles are presented in E direction (from the first gel layer to the pristine glass core) and L direction (from the pristine glass core to the second gel layer). Please refer to the methods section for more information.

Elements from the glass

The profile obtained for Zr^+ during analysis 1 is not perfectly flat (Fig. 1a), which is a result of the matrix effect. The other profiles displayed in Figure. 1 are devoid of these matrix effects due to Zr^+ normalization.[52] Al^+ profile displays a very similar shape as that of Zr^+ (Supplementary Material Fig. S1a), and as a result Al^+ normalized profile is perfectly flat (Fig. 1c)[28].Si^+ profile appears to vary lightly in shape compared to that of Zr^+ and Al^+ (Supplementary Material Fig. S1a), and its normalized profile does not appear to be perfectly flat (Supplementary Material Fig. S1c). At first impression, one could be tempted to say that the gel layer is faintly depleted in Si due to acid leaching conditions undergone by the flake sample. However, when comparing $^{28}Si^+$ profile with that of $^{29}Si^+$ and $^{30}Si^+$ (Supplementary Material Fig. S2a) it appears that $^{29}Si^+$ and ^{30}Si profiles are similar to that of Zr^+. Moreover, the $^{29}Si^+/^{28}Si^+$ and $^{30}Si^+/^{28}Si^+$ ratios in the both gel layers are slightly above that of natural abundance found in the pristine glass, while the $^{30}Si^+/^{29}Si^+$ one stays constant (Supplementary Material Fig. S2b). Considering that no enrichment of ^{29}Si nor ^{30}Si was brought by the solution, it is thus possible to affirm that the $^{28}Si^+$ profile shape is abnormal due to saturation effect of the detector. Therefore, the Si profiles presented here (Fig. 1b) is that of $^{29}Si^+$. Like Al^+[29],Si^+ normalized profile is flat, which is consistent with previous studies.[27,40,53]

Normalized B^+, Na_2^+, and Ca^+ concentrations drop from a value of 1 in pristine glass to a value below 0.15 in gel layers, and the sharp drop in the concentration of those three elements occurs at the same position, meaning that these elements were congruently dissolved under the studied conditions (Fig. 1d–f). All these results are also coherent with previous studies.[27,40,53]

The E and L profiles for normalized $^{29}Si^+$ and Al^+ are identical, meaning that these profiles, often displayed and discussed in the literature, were not affected by ion beam sputtering artifacts (Fig. 1b, c).[27,28,30,42] This is coherent with their role of glass former making covalent bonds with O atoms. B, while being a network former, is also known to be preferentially leached out even in Si-saturated conditions.[27,53] As for Na^+ and Ca^+, they are known to act mostly as charge compensators for $[BO_3]^-$, $[AlO_4]^-$, and $[ZrO_6]^{2-}$ units in ISG glass, and, to a lesser extent, as glass modifiers.[54] As these cations are less strongly bonded to the structure than the glass formers, their distributions within the gel could be impacted by the O or Cs beam. B^+ and Ca^+ profiles appear to be fairly symmetrical (Fig. 1d, f), but the same plots in logarithm scale (Supplementary Material Fig. S3a,b) reveal that both elements are slightly pushed forward, as a slight tail can be observed in the L direction. Na^{2+} profile is not symmetrical at all and displays differences in both shape and width at the pristine glass/gel interface (Fig. 1e). When analyzed in the E direction, the Na_2^+ interface is very sharp, similar to a Heaviside step function. On the contrary, when analyzed in the L direction, the Na profile is larger with a decrease in the Na_2^+ concentration in the pristine glass and a tail in the gel layer (Fig. 1e). Alkali profiles can be distorted when analyzing insulating materials due to the formation of an electric field.[1,55] Here, a low-energy electron flux was used to neutralized the surface of the sample in order to avoid such artifact. Notwithstanding, the shape of Na_2^+ L profile is not surprising. The difficulty to observe the diffusion of an element from a layer 1 to a layer 2 when the element is present at high concentration in layer 1 and as a trace in layer 2 is the reason backside analyses were developed in the first place.[56,57] However, it shows the tendency of some elements to be pushed forward by the ion beam in normal analysis condition. Na in particular is the most impacted, which is consistent with its ionization yield that is higher than that of B and Ca.

Exogenous species

All the exogenous species studied here (i.e., K^{18},O, and H) are assumed to be mostly mobile inside the gel structure. K is known to exchange with Ca as a charge compensator for $[AlO_4]^-$ and $[ZrO_6]^{2-}$ units.[53] Concerning ^{18}O and H, some uncertainties currently remain as to whether water molecules diffuse as such, or dissociate into H and O that then diffuse separately.[58] The H profile tends to be shifted compared to the ^{18}O profile, which could be an indication that water molecules dissociate and then react with the silicate network. It is reported that H profile also tends to be shifted compared to other species profiles (e.g., B, Na), which may indicate that hydration precedes ion exchange.[42]

Here[41],K^+ seems to have been pushed forward by the sputtering beam; its profile in the E direction is very sharp and anti-correlated with that of B^+, while it is shifted by ~70 nm in the

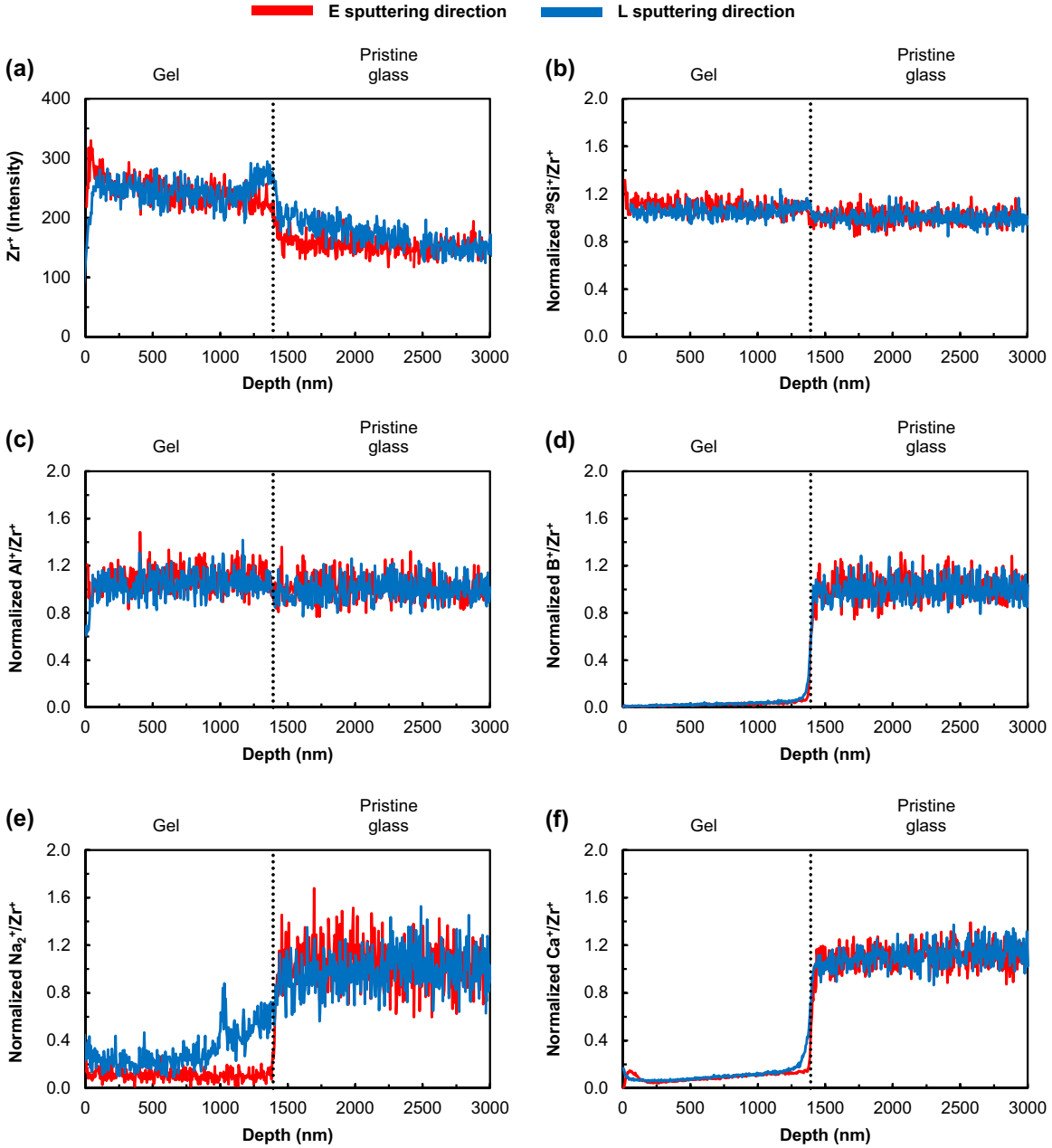

Fig. 1 Analysis 1 performed on the flake sample. Profiles of the glass cations. All profiles (except the Zr^+ one) are normalized to that of Zr^+, and the resulting data are normalized to the mean value found in the pristine glass. The position of the pristine glass/gel interface, determined from B^+ profiles, is represented by a black dotted line in each graph. **a** Zr^+ profile, **b** Si^+/Zr^+, **c** Al^+/Zr^+, **d** B^+/Zr^+, **e** $Na_2{}^+/Zr^+$, and **f** Ca^+/Zr^+ normalized profiles

L direction (Fig. 2b). Moreover, the shape of the $^{41}K^+$ profile differs depending on the sputtering direction; the enrichment in the interfacial area in E layer corresponds to a depletion in the same area of L layer (in blue).

Regarding ^{18}O and H, our results confirm that these elements were not pushed forward by the sputtering beam despite being fairly mobile elements[59]; their profiles widths at the interface are similar regardless of the sputtering direction (Fig. 2d, f). This validates the determination of the diffusion coefficient from the width of the H interface.[42] Moreover, H^- profiles are perfectly correlated with the $^{18}O^-$ profile and anti-correlated with the BO^{2-} profiles (Supplementary Material Fig. S4c, d), regardless of the sputtering direction, proving that, in the studied conditions, H does not diffuse inside the pristine glass as a separate proton species.

Still, the E layer seems to be slightly more depleted in both ^{18}O and H. Depletion in ^{18}O can be attributed to exchange with the moisture of the atmosphere during the sample preparation and handling, as the surface of the E layer remained in contact with air for 3 min before being introduced into the vacuum chamber.[59] However, as H was similarly impacted as ^{18}O, this could be the result of the vacuum needed for ToF-SIMS profiling (1.3×10^{-8} mbar) that leads to some confined water in the sample evaporation. The depletion in E layer is on a similar order of magnitude within experimental error for both H and ^{18}O (Table 1). H^- and $^{18}O^-$ profiles display similar shapes near the pristine glass/gel interface.

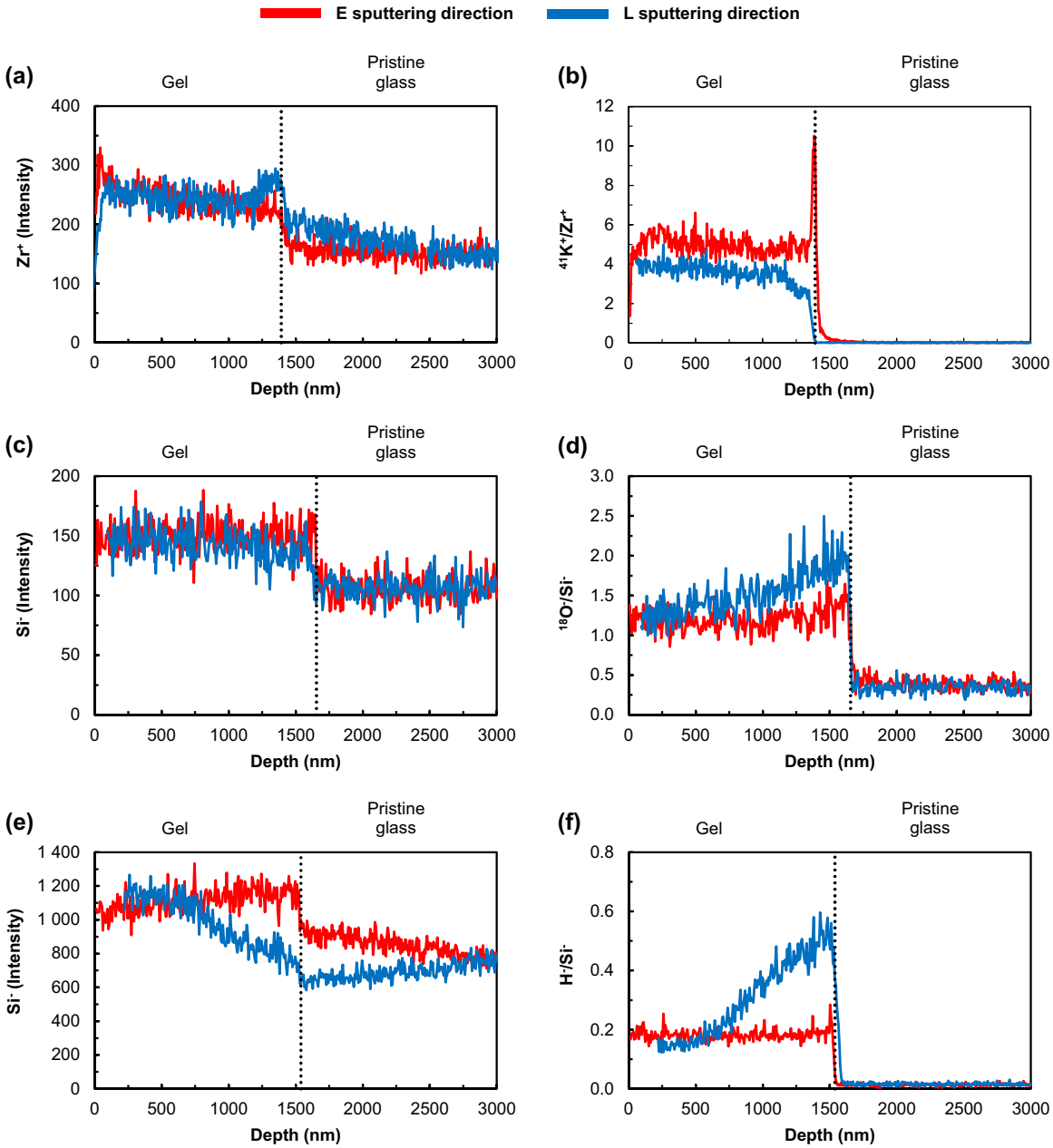

Fig. 2 Analysis 1, 2, and 3 performed on the flake sample. Profiles of exogenous elements and $^{18}O^{41}.K^{+}$ profile is normalized to that of Zr^{+}. H^{-}, and $^{18}O^{-}$ profiles are normalized to that of their respective Si^{-} profiles. The position of the pristine glass/gel interface, determined from B^{+} (Fig. 1d) and BO^{2-} profiles (Supplementary Material Fig. S4a, b), is represented by a black dotted line in each graph. **a** Zr^{+} profile from analysis 1, **b** $^{41}K^{+}/Zr^{+}$ profile (analysis 1), **c** Si^{-} profile from analysis 2, **d** $^{18}O^{-}/Si^{-}$ profile (analysis 2), **e** Si^{-} profile from analysis 3, and **f** H^{-}/Si^{-} profile (analysis 3)

Table 1. Comparison between data obtained in E and L layer

	H/Si	$^{18}O/Si$
E layer	0.18 ± 0.02	1.21 ± 0.15
L layer	0.31 ± 0.13	1.52 ± 0.27
Ratio (E layer/L layer)	0.60 ± 0.27	0.79 ± 0.16

However, H^{-} is slightly more depleted than $^{18}O^{-}$, especially near the external part of the gel (see the red dashed line in Fig. 3). This suggests that H could have diffused toward the carbon tape as a proton, as proved by the enrichment of H when reaching the flake/carbon tape interface (Supplementary Material Fig. S5).

Analysis of the monolith samples

The previous observations suggested that the sputtering beam does not impact network formers such as Si and Al, but could push forward some mobile species such as B, K, Na, and Ca. This could reduce the interfacial profile width usually presented in the literature (profiles obtained in the E direction) and, in turn, lead to some uncertainties regarding the profile shapes at the pristine glass/gel interfaces. To further investigate this idea, the choice was

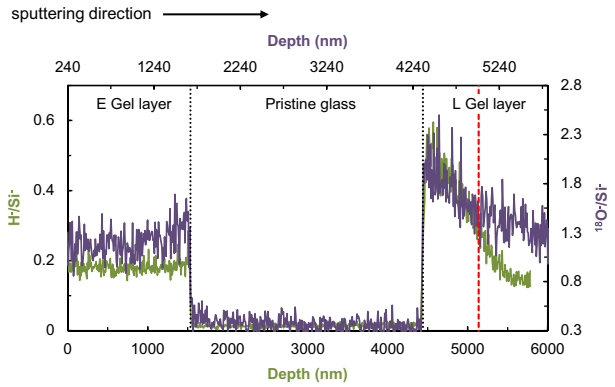

Fig. 3 Analysis 2 and 3 performed on the flake. H^- and $^{18}O^-$ profiles normalized to that of their respective Si^- profiles. Those data are similar to that presented in Fig. 2b, c, but are plotted as a function of total depth of the sample. The position of the pristine glass/gel interfaces, determined from BO^{2-} profiles (Supplementary Material Fig. S4c, d), is represented by black dotted lines. The red dashed line indicates the depth at which the profiles shapes differ

made to analyze two similar samples with and without cryo-treatment, prior to the ToF-SIMS analysis. Cryo-treatment has previously been used to study the migration of alkalis in thin SiO_2 layers,[60] showing drastic differences between alkalis profiles at ambient temperature and low temperatures (down to −120 °C).

Despite being altered in the same vessel, the monoliths used for cryo- and non-cryo-analysis do not display the same alteration depth (~545 nm and ~860 nm, respectively). However, it has been previously demonstrated above and in other studies that the layer formed in Si-saturated conditions are homogeneous.[27,40,53] It means that while they have different alteration depths, both monoliths should display similar profiles for each elements. Indeed, all network former profiles, including that of B, are similar (Supplementary Material Fig. S6a to d) and can be perfectly superimposed when aligning the pristine glass/gel interfaces (Supplementary Material Fig. S6e to g). However, the cryo-treatment is expected to reduce the mobility of the cation species. Here, the differences observed between the cryo- and non-cryo-profiles suggest that some cations were impacted (Fig. 4), although the resulting effect differs depending on their origin (from the pristine glass or from the solution).

Na and Ca are two elements that come from the pristine glass and are depleted inside the gel layer. Na_2^+ profiles are fairly similar in shape, even if the cryo profile is slightly above its non-cryo counterpart (Fig. 4a). This element does not appear to be much pushed forward in this experiment. Ca^+ profiles, on the contrary, differ depending on the thermal treatment of the sample (Fig. 4b). Ca amount rises linearly in the cryo profile (from 0.20 to 0.45 after the initial bump) until it reaches a fairly narrow pristine glass/gel interface. For the non-cryo experiment, Ca^+ amount also rises linearly, although with a greater slope (from 0.00 to 0.70), and the interface is less pronounced. This suggest that the sputtering beam pushes Ca atoms forward, a result that is more visible than in the previous experiment on the flake sample because of Ca higher mean concentration inside the gel layer.

Profiles obtained for exogenous species such as Li, K, and Cs also differ depending on the sample treatment. The non-cryo-profiles of these species display an artificial defect with a decreasing slope and a shape that is less flat than its cryo-counterpart. This artifact is more pronounced for light elements such as Li and K, and nearly nonexistent for Cs, proving that heavy elements were less displaced by the ion beam due to reduced mobility in this type of material. These results are consistent with that obtained by Krivec, et al.[60] in thin SiO_2 layer. In addition, one might note that Li cryo profile is still less flat than that of other alkalis, suggesting that this light element might still be pushed forward by the beam despite the cryo-treatment, as previously observed by Krivec, et al.[60]. All Li^+ and $^{41}K^+$ profiles show a dramatic enrichment at the pristine glass/gel interface, which suggest that this is an actual feature of this type of gel layer. It can be explained by the fact that this area was still very reactive, with negatively charged boron units still requiring charge compensation. The rest of the gel layer, which has had some time to reorganize, was completely boron-depleted and globally homogeneous in composition, explaining why the cation profiles are mostly flat.[59] However, the absence of this enrichment in the cryo experiment for Cs_2^+—the less impacted alkali—profile raises uncertainties on this affirmation. The enrichment observed for Li^+ and $^{41}K^+$ could still be an artifact of the ion beam even during cryo experiments, as observed by Krivec, et al.[60] This needs to be further studied.

In this type of material (nanoporous gel layer formed in Si-saturated conditions), previous cryo experiments suggested that no water evaporation was caused by the ToF-SIMS vacuum.[59] The results obtained here do not allow us to draw any further conclusions regarding H_2O evaporation caused by the ToF-SIMS vacuum (1.3×10^{-8} mbar). While the H/Si value is higher in the cryo experiment, the ^{18}O/Si value is lower (Fig. 5, Table 2). To address this apparent contradiction, further investigation with model porous materials is needed. Nevertheless, the value found for each elements are close enough that it is possible to rule out any significant water evaporation due to the vacuum.

$^{18}O/^{16}O$ profiles

During this study, especially for the flake sample where a low $^{18}O^-$ signal was expected, our analytical conditions were adjusted to optimize the sensitivity of ^{18}O measurement. However, this was done to the detriment of ^{16}O measurement, resulting in a saturated non-linear response of the detector. This makes the determination of the isotopic ratio impossible for our samples: values that differ from the natural abundance for the $^{18}O/^{16}O$ ratio are found inside the pristine glass (up to 3.7-fold higher, Fig. 6). ToF-SIMS lower sensitivity compared to that of D-SIMS thus constrain the domain of isotopic enrichment that can be use if quantities data are required: a too low enrichment for the minor isotope is not favorable, as the adjustment of the detector often lead to saturation effect for the major isotope.

In summary, our study demonstrates that, despite careful sample preparation and analysis, ToF-SIMS data could be incorrectly interpreted due to several analytical artifacts. This should be considered in future studies on glass corrosion, as well as any other studies considering material corrosion and/or tracing experiments. Some caveats from this study are:

- Sample preparation, and most notably the sample holder chosen (carbon tape) can contaminate and/or affect the chemistry of the sample. We have seen here for example that H migrates toward the carbon tape.
- Ion sputtering can affect the shape and the position of cation depth profiles and lead to incorrect interpretations regarding alteration layer formation. These effects, once known, can be better controlled by using cryo-treatment or backside analysis for example, or by adjusting the ToF-SIMS analysis conditions (charging effect can be avoided using a charge neutralization device for example). For light mobile elements such as Li and Na, one must consider using a O^- sputter ion beam coupled with an offset voltage applied to the surface of the glass for continuous correction of the charge.
- Sample roughness can also affect the mass spectrum, and impact the depth profile shapes, especially at the pristine glass/gel interface.[42] The size of both the ion sputtered area

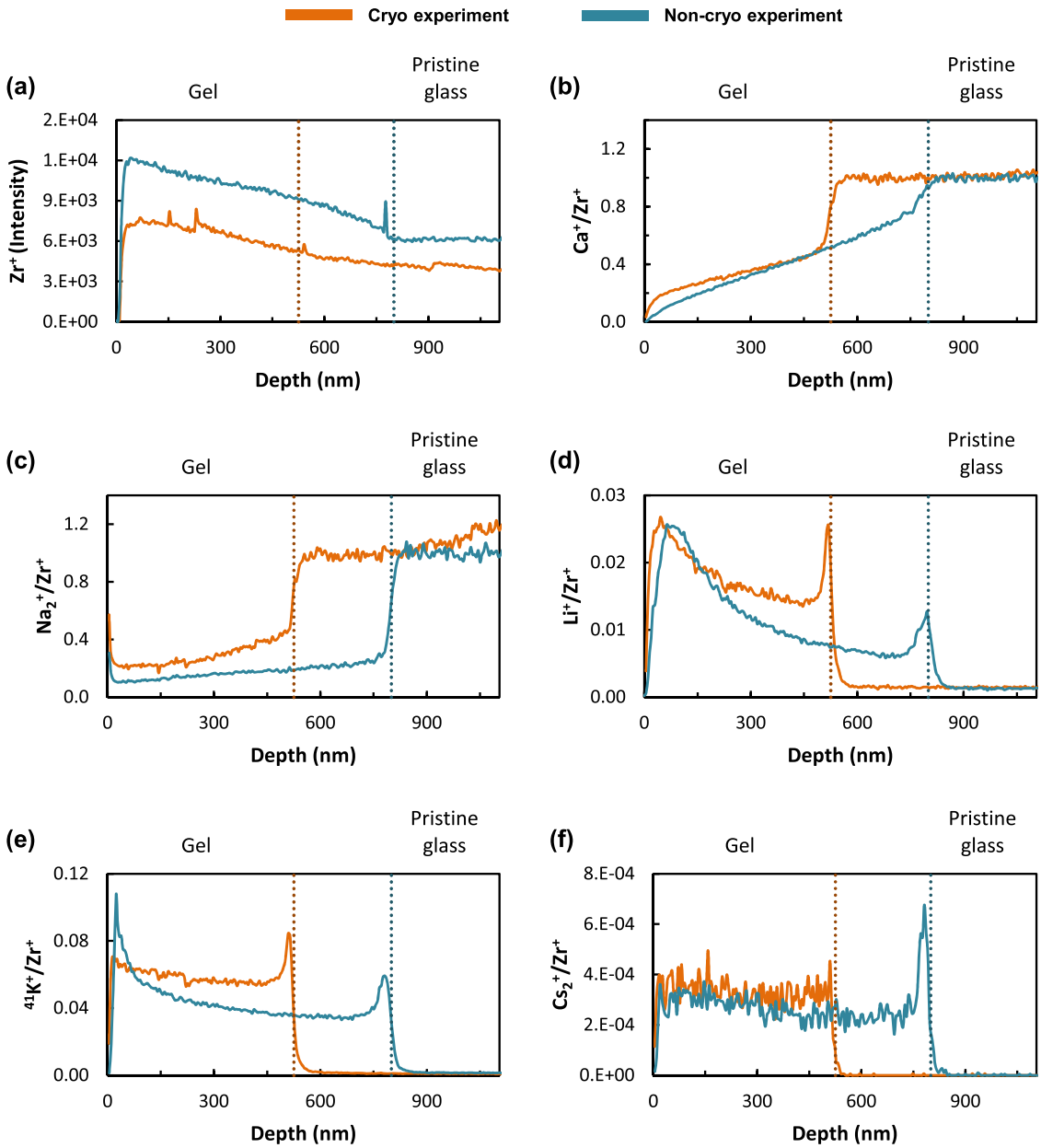

Fig. 4 Profiles obtained on the monolith samples. The positions of the pristine glass/gel interfaces, determined from the B^+ profile (Supplementary Material Fig. S6c), are represented by vertical dotted lines. The profiles displayed are those of **a** Zr^+, **b** Ca^+/Zr^+, **c** Na_2^+/Zr^+, **d** Li^+/Zr^+, **e** $^{41}K^+/Zr^+$, and **f** Cs_2^+/Zr^+. For Ca and Na, the data resulting from Zr^+ normalization are normalized to the mean value found in the pristine glass

and the analyzed area, as well as their position on the sample have to be chosen carefully to reduce uncertainties.

- ToF-SIMS can be quantitative by the use of isotopic ratios of exogenous tracing elements (e.g., D/H^{18},$O/^{16}O^{29}$,$Si/^{28}Si$), provided that the enrichment of the minor isotope is sufficient to give a measurable signal for the major isotope. Some recent studies have also pushed for access to quantitative data for other exogenous elements, such as H, using standard values.[13,61,62] This is of great interest for corrosion study, regardless of the material studied.
- While ToF-SIMS data are usually presented as a function of depth, one must keep in mind that abrasion rates might differ from one layer to another. For the glass alteration study, the same abrasion rate was considered for the gel layer and the pristine glass, but secondary phases are known to be abraded faster than other layers.[15] This should be verified prior to analysis.
- Finally, in this study, water evaporation due to low pressure in the ToF-SIMS chamber was observed. However, in this case the effect seems small as the material studied (gel layer formed on pristine glass) is nanoporous with a low amount of open pores. Larger evaporation might be expected for highly hydrated samples exhibiting a larger-sized porosity and a greater open porosity. In such a case, one might consider specific sample preparation prior to analysis, such as cryo-preparation and the use of a cooled stage during the analysis.

METHODS

Sample preparation

The experiments were performed on an ISG batch whose composition is detailed in Table 3, prepared by MoSci Corporation (Rolla, MO, USA).[27] The

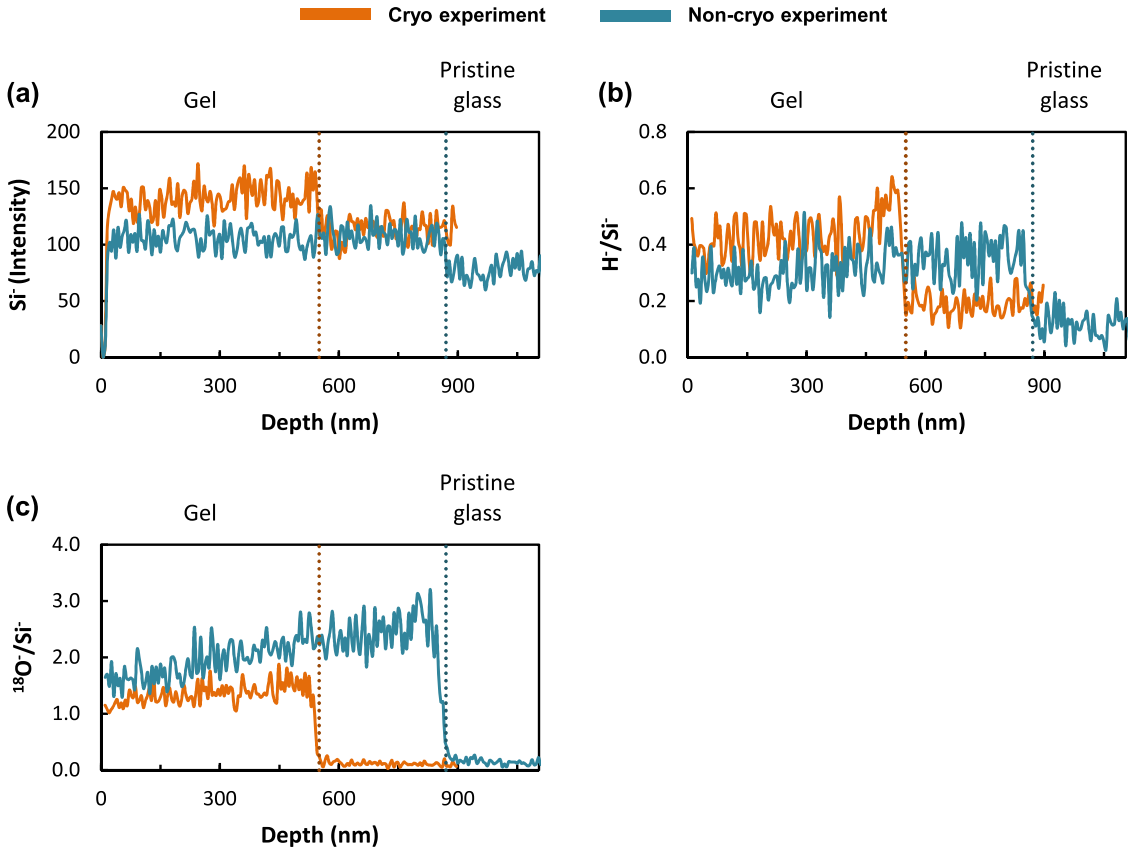

Fig. 5 Profiles obtained on the monolith samples. The positions of the pristine glass/gel interfaces, determined from the BO^{2-} profile (Supplementary Material Fig. S4e), are represented by vertical dotted lines. The profile displayed are those of **a** Si^-, **b** H^-/Si^-, and **c** $18\,O^-$

Table 2. Comparison between data obtained on monolith samples with different heat treatment

	H/Si	^{18}O/Si
Non-cryo experiment	0.32 ± 0.07	2.04 ± 0.34
Cryo experiment	0.42 ± 0.07	1.33 ± 0.15
Ratio (Non-cryo/Cryo)	0.76 ± 0.16	1.53 ± 0.25

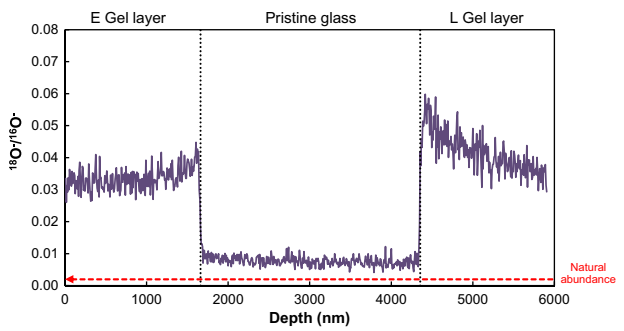

Fig. 6 $^{18}O^-/^{16}O^-$ profiles. Results obtained on the flake sample (Analysis 2). The experimental value obtained in the pristine glass is higher than that expected. The position of the pristine glass/gel interfaces, determined from the BO^{2-} profiles (Supplementary Material Fig. S4c), is represented by black dotted lines. The red dashed line represents the natural abundance

Table 3. ISG glass composition

ISG						
Oxides	SiO_2	B_2O_3	Na_2O	Al_2O_3	CaO	ZrO_2	
wt%	56.1	17.3	12.2	6.1	5.0	3.3	
mol%	60.1	16.0	12.6	3.8	5.7	1.7	
Element	Si	B	Na	Al	Ca	Zr	O
wt%	26.3	5.4	9.0	3.2	3.6	2.4	50.1
At%	18.0	9.6	7.6	2.3	1.7	0.5	60.3

ISG glass powder was melted at ~1400 °C. A piece of molten glass was then blown against a flat graphite bar. This protocol provided several flat flakes of a few square millimeters in area and a thickness ranging from 5 to 10 µm. Figure 7 shows an SEM image of such a flake. The selected one was ~6 µm thick. Two monoliths measuring (0.5 × 0.5 × 0.2) cm^3 each were also prepared and polished to 1 µm on the two largest sides.

Leaching experiment

A roughly 6 µm thick flake was altered at 90 °C in a PFA vessel for 29 h in a solution containing 160 $mg{\cdot}L^{-1}$ of Si (saturation with amorphous SiO_2), and 2 $g{\cdot}L^{-1}$ of K. The pH at 90 °C was maintained at around 5.5. When removed from the leaching solution, the glass flake was quickly rinsed with deionized water and then placed for 3 h at room temperature in an isotopically spiked solution prepared with $H_2{}^{18}O$ (over 97% of ^{18}O). The expected value for $^{18}O/^{16}O$ in this solution (2.4 ± 0.2), based on the weighting of the chemicals, was verified by direct measurement. For that, the solution was first equilibrated with $^{12}C^{16}O_2$, so that:

$$^{12}C^{16}O_2 + H_0^{18}OD^{12}C^{16}O^{18}O + H_2^{16}O \quad (1)$$

After 15 h of contacting time at room temperature, the CO_2 gas was analyzed with a direct inlet mass spectrometer with magnetic sector and Faraday cup detector (to provide flat top peaks with good quantification). Intensities measurement on masses 44, 45, 46, 47, 48, and 49 provided oxygen isotopic ratio. The obtained value, 2.29 ± 0.04, is close to the expected one. This verification is highly recommended for the quantification of water exchange in porous samples, especially when working at high enrichment. The calculated $^{18}O/^{16}O$ approach infinity when the percentage of ^{18}O in solution increases toward 100 (Supplementary Material Fig. S7). While no quantification calculation done here neither for the flake sample nor the monoliths sample data (analytical conditions used prevented the acquisition of isotopic ratio), it is a useful tool that is currently being developed to better understand gel passivating properties.[59]

To study the potential interaction between the ToF-SIMS sputter ion beam and alkali metals, as well as ^{18}O, the two large monoliths ((0.5 × 0.5 × 0.2) cm^3 each) were altered in a PFA vessel at 90 °C for three days in a solution containing 160 mg·L^{-1} of Si (saturation with amorphous SiO_2). The pH at 90 °C was maintained around 7. After three days, the monoliths were traced for 24 h in a solution enriched in ^{18}O ($^{18}O/^{16}O = 1.1$) containing 1.8, 2.7, 3.7, and 7.2 g·L^{-1} of LiCl, NaCl, KCl, and CsCL, respectively, before ToF-SIMS analysis was conducted.

These leaching conditions (pH near neutral, concentration of Si near saturation with respect to amorphous silica) enable the formation of an amorphous passivating layer of constant thickness on the surface with no secondary phases.[27,40]

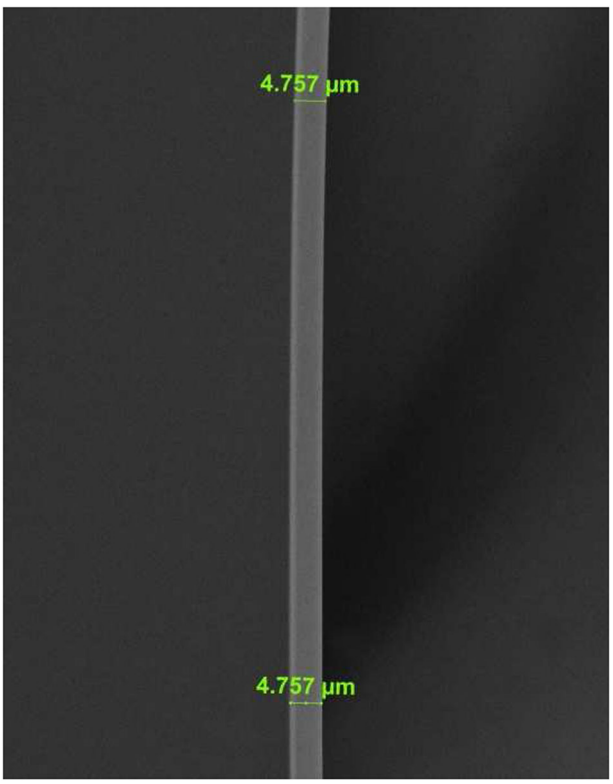

Fig. 7 SEM image taken on the edge of a pristine flake of ISG glass

ToF-SIMS analysis

The flake sample was retrieved from the tracing solution of $H_2{}^{18}O$ and directly placed on carbon tape without drying. It was then mounted onto the sample holder and then quickly introduced into the vacuum chamber (1.3×10^{-8} mbar) of the SIMS (IONTOF TOF 5) to limit isotopic exchange with air. The monolith samples were each retrieved from their alteration solution and quickly blow-dried with dry air. One sample was directly mounted onto the sample holder and introduced into the vacuum chamber of the SIMS. The other sample was placed in liquid nitrogen (77 K) for 3 h before being mounted onto a cooled sample holder and introduced into the vacuum chamber of the SIMS. In this case, the analysis was performed at a temperature around 120 K. The external face of each sample remained in contact with air for ~3 h. Three profiles were recorded for each sample, as described in the table below. Glass being a known insulator, the sample surface was neutralized during analysis by a low-energy electron flux (<20 eV).[63] The analytical conditions are reported in Table 4.

The depth calibration was conducted based on the thickness of the flake sample (~6 µm) or determined using a profilometer to measure the crater depth at the end of the analysis of the monolith samples. However, it has to be noted that the flake sample tended to crack at the end of each SIMS analysis, meaning that there are some uncertainties regarding the last tens of nanometer of the profiles. The same abrasion rate was assumed for gel and pristine glass.[27] In the case of analysis 1, exogenous elements profiles were normalized to that of Zr to limit matrix effects (see Supplementary Material Fig. S8a for a comparison between ^{28}Si raw profiles for analyses 1, 2, and 3). Zr was chosen as it remained undissolved and, thus, immobile during the experiment.[52]

$$C(i) = \frac{i}{Zr} \text{ with } i = \text{Li, K, and Cs.} \quad (2)$$

With regard to the elements present in the pristine glass, all profiles were normalized to that of Zr, and then, the resulting data were normalized to the mean value measured in the pristine glass using the following formula:

$$C(i) = \frac{[i/Zr]}{[i/Zr]_{\text{pristine glass}}} \text{ with } i = \text{Si, Al, B, Na, and Ca.} \quad (3)$$

Because Zr was not detected in analysis 2 and 3, the concentrations were normalized to that of ^{28}Si to limit the matrix effect. Si is not mobile in the present conditions, and Si^+ normalization yield the same results as Zr^+ normalization in analysis 1 (Supplementary Material Fig. S8b).[27]

$$C(i) = \frac{i}{Si} \qquad \text{with } i = \text{B, H, and } ^{18}\text{O.} \quad (4)$$

Note that due to detector saturation, $Na_2{}^{+41}$,K^+, and $Cs_2{}^+$ profiles were preferred over Na^{+39},K^+, and Cs^+ profiles, while $^6Li^+$ and $^7Li+$ profiles are similar (Supplementary Material Fig. S9a to j).

The small thickness of the flake sample allowed its analysis to take place from one face to the other, meaning that the two gel layers formed during alteration and the pristine layer remaining in the middle were characterized by the analysis (Fig. 8a). Gel layer 1 was analyzed in the entering sputtering direction (gel to pristine glass), while gel layer 2 was analyzed in the leaving sputtering direction (pristine glass to gel). In this article, the entering sputtering direction (red arrow) is called E, and the leaving sputtering direction (blue arrow) is called L for simplification. The profiles recorded were assumed to be perfectly symmetrical (Fig. 8b),

Table 4. Experimental conditions for the three analysis performed

Sample	Type of analysis		Analysis beam	Abrasion beam	Sputtered area	Analyzed area	Elements of interest
Flake sample	Analysis 1	Positive secondary ions	$Bi_1{}^+$ 25 keV I ~2 pA	$O_2{}^+$ 1 keV 220 nA	200 × 200 µm²	50 × 50 µm²	Si, B, Na, Al, Ca, Zr, K
	Analysis 2	Negative secondary ions	$Bi_3{}^{++}$ 25 keV I = 0.06 pA	Cs^+ 2 keV 210 nA	200 × 200 µm²	50 × 50 µm²	B^{16}, O^{18}, O, Si
	Analysis 3	Negative secondary ions	$Bi_1{}^+$ 25 keV I = 1.8 pA	Cs^+ 2 keV 210 nA	200 × 200 µm²	50 × 50 µm²	B, H, Si
Monoliths	Analyses 4	Positive secondary ions	$Bi_1{}^+$ 25 keV I ~1.5 pA	$O_2{}^+$1 keV 180 nA	200 × 200 µm²	50 × 50 µm²	Si, B, Na, Al, Ca, Zr, K
	Analyses 5	Negative secondary ions	$Bi_3{}^{++}$ 25 keV I = 0.03 pA	Cs^+ 2 keV 150 nA	200 × 200 µm²	50 × 50 µm²	B^{16}, O^{18}, O, Si

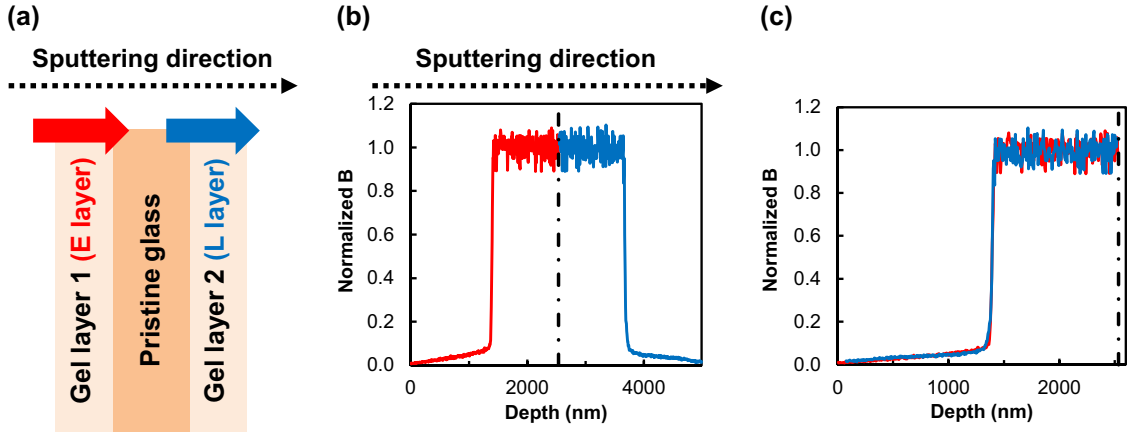

Fig. 8 **a** Schematic representation of the ToF-SIMS analysis performed on the glass flake. E and L stand for entering and leaving respectively, and indicate the sputtering direction. **b** Full profile obtained (here for B^+ or B^-) with the symmetry outlined in black. **c** Comparison between the two parts of the profile

meaning that the second part of the profile can be reversed and then superimposed onto the first part (Fig. 8b). The shape and width of the two profiles were then compared to discuss potential artifacts. Boron was used to determine the position of the symmetric axis for all the other profiles.

In the case of the monolith samples, the profiles were expected to be exactly similar in depth, as both samples were altered at the same time. However, due to experimental conditions (very first days of alteration in Si-saturated condition), this was not the case—the sample analyzed with cryo-treatment has a mean gel thickness of ~535 nm while the one analyzed without cryo-treatment has a mean thickness of ~860 nm.

DATA AVAILABILITY

The data that support the findings of this study are available from the corresponding author upon reasonable request.

ACKNOWLEDGEMENTS

This work was supported as part of the Center for Performance and Design of Nuclear Waste Forms and Containers, an Energy Frontier Research Center funded by the U.S. Department of Energy, Office of Science, Basic Energy Sciences under Award # DE-SC0016584. The authors are grateful to Loïc Marchetti, Magaly Tribet, and Sylvain Peuget for scientific input, and to Manon Cornaton for performing the analysis of the oxygen isotopic ratio in the tracing solution.

AUTHOR CONTRIBUTIONS

M.C. was responsible for some experimental analyses and for writing the paper. S.G. and P.J. supervised the study and performed the experiment with the glass flake. L.D. (Tescan Analytics) performed the ToF-SIMS analyses. V.D. was responsible for the analysis of the oxygen isotopic ratio in the tracing solution. L.D. (PRIME Verre) prepared the glass flakes. All the authors helped on paper editing.

ADDITIONAL INFORMATION

Supplementary information accompanies the paper on the *npj Materials Degradation* website (https://doi.org/10.1038/s41529-019-0076-3).

Competing interests: The authors declare no competing interests.

Publisher's note: Springer Nature remains neutral with regard to jurisdictional claims in published maps and institutional affiliations.

REFERENCES

1. Deloule, E. & Valle, N. Trace element and isotope analysis using secondary ion mass spectrometry. *Eur. Mineral. Union Notes Mineral.* **16**, 131–164 (2017).
2. Wilson, R. G., Stevie, F. A. & Magee, C. W. *Secondary Ion Mass Spectrometry: A Practical Handbook for Depth Profiling and Bulk Impurity Analysis*. (Wiley, New Jersey, 1989).
3. Szynkowska, M. I., Czerski, K., Rogowski, J., Paryjczak, T. & Parczewski, A. ToF-SIMS application in the visualization and analysis of fingerprints after contact with amphetamine drugs. *Forensic Sci. Int.* **184**, e24–26 (2009).
4. Gazi, E. et al. The combined application of FTIR microspectroscopy and ToF-SIMS imaging in the study of prostate cancer. *Farad. Disc.* **126**, 41 (2004).
5. Youn, S. C. et al. Comprehensive application of time-of-flight secondary ion mass spectrometry (TOF-SIMS) for ionic imaging and bio-energetic analysis of club drug-induced cognitive deficiency. *Sci. Rep.* **5**, 18420 (2015).
6. Bulle-Lieuwma, C. W. T. et al. Characterization of polymer solar cells by TOF-SIMS depth profiling. *Appl. Surf. Sci.* **203–204**, 547–550 (2003).
7. Engrand, C. et al. Chemometric evaluation of time-of-flight secondary ion mass spectrometry data of minerals in the frame of future in situ analyses of cometary material by COSIMA onboard ROSETTA. *Rapid Commun. Mass Spectrom.* **20**, 1361–1368 (2006).
8. Vickerman, J. C. & Briggs, D. *ToF-SIMS: Materials Analysis by Mass Spectrometry*. 2nd edn (IM Publications, UK, 2013).
9. Neeway, J. J. et al. Low-temperature lithium diffusion in simulated high-level boroaluminosilicate nuclear waste glasses. *J. Non Cryst. Solids* **405**, 83–90 (2014).
10. Chave, T., Frugier, P., Gin, S. & Ayral, A. Glass-water interphase reactivity with calcium rich solutions. *Geochim. Cosmochim. Acta* **75**, 4125–4139 (2011).
11. Ducasse, T. et al. Alteration of synthetic basaltic glass in silica saturated conditions: analogy with nuclear glass. *Appl. Geochem.* **97**, 19–31 (2018).
12. Mougnaud, S. et al. Heavy ion radiation ageing impact on long-term glass alteration behavior. *J. Nucl. Mater.* **510**, 168–177 (2018).
13. Zhu, Z., Shutthanandan, V. & Engelhard, M. An investigation of hydrogen depth profiling using ToF-SIMS. *Surf. Interface Anal.* **44**, 232–237 (2012).
14. Zhang, J. et al. Nanoscale imaging of alteration layers of corroded international simple glass particles using ToF-SIMS. *Nucl. Instrum. Methods Phys. Res. Sect. B* **404**, 45–51 (2017).
15. Aréna, H. et al. Impact of Zn, Mg, Ni and Co elements on glass alteration: additive effects. *J. Nucl. Mater.* **470**, 55–67 (2016).
16. Verney-Carron, A., Saheb, M., Loisel, C., Duhamel, R. & Remusat, L. Use of hydrogen isotopes to understand stained glass weathering. *Procedia Earth Planet. Sci.* **13**, 64–67 (2015).
17. Alloteau, F. et al. New insight into atmospheric alteration of alkali-lime silicate glasses. *Corros. Sci.* **122**, 12–25 (2017).
18. Walton, A. W., Schiffman, P. & Macpherson, G. L. Alteration of hyaloclastites in the HSDP 2 Phase 1 Drill Core: 2. Mass balance of the conversion of sideromelane to palagonite and chabazite. *Geochem. Geophy. Geosy.* **6**, 9 (2005).
19. Grambow, B. Nuclear waste glasses—how durable? *Elements* **2**, 357–364 (2006).
20. Poinssot, C. & Gin, S. Long-term behavior science: the cornerstone approach for reliably assessing the long-term performance of nuclear waste. *J. Nucl. Mater.* **420**, 182–192 (2012).
21. Corrêa Pinto, A. M., Macedo, M. F. & Vilarigues, M. G. The conservation of stained-glass windows in Latin America: A literature overview. *J. Cult. Herit.* **34**, 172–181 (2018).
22. Murcia-Mascarós, S. Glass science in art and conservation. *J. Cult. Herit.* **9**, e1–e4 (2008).
23. Angeli, F., Jollivet, P., Charpentier, T., Fournier, M. & Gin, S. Structure and chemical durability of lead crystal glass. *Environ. Sci. Technol.* **50**, 11549–11558 (2016).

24. Palomar, T., de la Fuente, D., Morcillo, M., Alvarez de Buergo, M. & Vilarigues, M. Early stages of glass alteration in the coastal atmosphere. *Build. Environ.* **147**, 305–313 (2019).
25. Hristova, Y., Djambaski, P., Samuneva, B., Rangelova, N. & Bogdanova, S. Development of drug adsorbates onto soluble inorganic silicate glass surface: example with acetaminophen. *J. Mater. Sci. Mater. Med.* **19**, 805–811 (2008).
26. Verney-Carron, A. et al. Understanding the mechanisms of Si–K–Ca glass alteration using silicon isotopes. *Geochim. Cosmochim. Acta* **203**, 404–421 (2017).
27. Gin, S. et al. Origin and consequences of silicate glass passivation by surface layers. *Nat. Commun.* **6**, 6360 (2015).
28. Hellmann, R. et al. Unifying natural and laboratory chemical weathering with interfacial dissolution-reprecipitation: a study based on the nanometer-scale chemistry of fluid-silicate interfaces. *Chem. Geol.* **294–295**, 203–216 (2012).
29. Geisler, T. et al. The mechanism of borosilicate glass corrosion revisited. *Geochim. Cosmochim. Acta* **158**, 112–129 (2015).
30. Chave, T., Frugier, P., Ayral, A. & Gin, S. Solid state diffusion during nuclear glass residual alteration in solution. *J. Nucl. Mater.* **362**, 466–473 (2007).
31. Valle, N. et al. Elemental and isotopic (29Si and ^{18}O) tracing of glass alteration mechanisms. *Geochim. Cosmochim. Acta* **74**, 3412–3431 (2010).
32. Geisler, T. et al. Aqueous corrosion of borosilicate glass under acidic conditions: a new corrosion mechanism. *J. Non Cryst. Solids* **356**, 1458–1465 (2010).
33. Hellmann, R. et al. Nanometre-scale evidence for interfacial dissolution-reprecipitation control of silicate glass corrosion. *Nat. Mater.* **14**, 307–311 (2015).
34. Fournier, M., Frugier, P. & Gin, S. Resumption of alteration at high temperature and pH: rates measurements and comparison with initial rates. *Procedia Mater. Sci.* **7**, 202–208 (2014).
35. Fournier, M., Gin, S. & Frugier, P. Resumption of nuclear glass alteration: State of the art. *J. Nucl. Mater.* **448**, 348–363 (2014).
36. Fournier, M., Gin, S., Frugier, P. & Mercado-Depierre, S. Contribution of zeolite-seeded experiments to the understanding of resumption of glass alteration.*npj Mater. Degrad.* **1**, 17 (2017).
37. Gin, S. et al. Nuclear glass durability: new insight into alteration layer properties. *J. Phys. Chem. C.* **115**, 18696–18706 (2011).
38. Sessegolo, L. et al. Long-term weathering rate of stained-glass windows using H and O isotopes. *npj Mater. Degrad.* **2**, 17 (2018).
39. Lenting, C. et al. Towards a unifying mechanistic model for silicate glass corrosion. *npj Mater. Degrad.* **2** (2018).
40. Collin, M. et al. Structure of international simple glass and properties of passivating layer formed in circumneutral pH conditions. *npj Mater. Degrad.* **2**, 4 (2018).
41. Gin, S. et al. The controversial role of inter-diffusion in glass alteration. *Chem. Geol.* **440**, 115–123 (2016).
42. Gin, S. et al. Atom-probe tomography, TEM and ToF-SIMS study of borosilicate glass alteration rim: a multiscale approach to investigating rate-limiting mechanisms. *Geochim. Cosmochim. Acta* **202**, 57–76 (2017).
43. Doremus, R. H. Interdiffusion of hydrogen and alkali ions in a glass surface. *J. Non-Cryst. Solids* **19**, 137–144 (1975).
44. Hellmann, R., Dran, J. C. & Della Mea, G. The albite water system: Part III. Characterization of leached and hydrogen - enriched layers formed at 300 °C using MeV ion Beam techniques. *Geochim. Cosmochim. Acta* **61**, 1575–1594 (1997).
45. Grambow, B. & Muller, R. First-order dissolution rate law and the role of surface layers in glass performance assessment. *J. Nucl. Mater.* **298**, 112–124 (2001).
46. Parruzot, B., Jollivet, P., Rebiscoul, D. & Gin, S. Long-term alteration of basaltic glass: mechanisms and rates. *Geochim. Cosmochim. Acta* **154**, 28–48 (2015).
47. Stevie, F. A., Garcia, R., Richardson, C. & Zhou, C. Back side SIMS analysis. *Surf. Interface Anal.* **46**, 241–243 (2014).
48. Hopstaken, M. J. P., Cabral, J. C., Pfeiffer, D., Molella, C. & Ronsheim, P. In *Proc. Frontiers of Characterization and Metrology for Nanoelectronics*. (American Institute of Physics, Melville, N.Y., 2009).
49. Hongo, C., Tomita, M., Takenaka, M. & Murakoshi, A. Accurate SIMS depth profiling for ultra-shallow implants using backside SIMS. *Appl. Surf. Sci.* **203–204**, 264–267 (2003).
50. Hongo, C., Takenaka, M., Kamimuta, Y., Suzuki, M. & Koyama, M. Backside-SIMS profiling of dopants in thin Hf silicate film. *Appl. Surf. Sci.* **231–232**, 594–597 (2004).
51. Gin, S. et al. An international initiative on long-term behavior of high-level nuclear waste glass. *Mater. Today* **16**, 243–248 (2013).
52. Cailleteau, C. et al. Insight into silicate-glass corrosion mechanisms. *Nat. Mater.* **7**, 978–983 (2008).
53. Collin, M., Fournier, M., Charpentier, T., Moskura, M. & Gin, S. Impact of alkali on the passivation of silicate glass. *npj Mater. Degrad.* **2**, 16 (2018).
54. Galoisy, L. et al. Evidence for 6-coordinated zirconium in inactive nuclear waste glasses. *J. Am. Ceram. Soc.* **82**, 2219–2224 (1999).
55. Migeon, H. N., Schumacher, M. & Slodzian, G. Analysis of insulating specimens with the Cameca IMfS. *Surf. Interface Anal.* **16**, 9–13 (1990).
56. Lareau, R. T., in Secondary Ion Mass Spectrometry, SIMS VI, (eds Benninghoven, I A., Huber, A. M. & Werner, H. W.) (J. Wiley, New York, 1988).
57. Palmstrom, C. J. et al. A high depth resolution backside secondary ion mass spectrometry technique used for studying metal/GaAs contacts. *Advanced Surface Processes for Optoelectronics: Symposium*. 283–288 (1988).
58. Doremus, R. H. Diffusion of water in rhyolite glass: diffusion-reaction model. *J. Non Cryst. Solids* **261**, 101–107 (2000).
59. Gin, S. et al. Dynamics of self-reorganization explains passivation of silicate glasses. *Nat. Commun.* **9**, 2169 (2018).
60. Krivec, S., Amsüss, A., Schwab, S. & Hutter, H. Diffrences between Li, Na, and K migration in SiO_2 films during ToF-SIMS O^{2+} depth profiling. *J. Vac. Sci. Technol. B* **36**, 1–5 (2018).
61. Kudriavtsev, Y., Asomoza-Palacio, R. & Manzanilla-Naim, L. Interaction of water vapor with silicate glass surfaces: Mass-spectrometric investigations. *Tech. Phys. Lett.* **43**, 447–449 (2017).
62. Kudriavtsev, Y., Asomoza-Palacio, R. & Manzanilla-Naim, L. New insight into water-obsidian interaction. *Revista Mexicana de Fisica* **63**, 19–25 (2017).
63. Hunt, C. P., Stoddart, C. T. H. & Seah, M. P. The surface analysis of insulators by SIMS: charge neutralization and stabilization of the surface pottential. *Surf. Interface Anal.* **3**, 147–160 (1981).